High injection rates counteract formation of far-reaching fluid migration pathways at The Geysers geothermal field

Stanislaw Lasocki[1,1] and Beata Orlecka-Sikora[2,2]

[1]Institute of Geophysics, Polish Academy of Sciences
[2]Institute of Geophysics Polish Academy of Sciences

November 30, 2022

Abstract

Deep underground water injections induce seismicity. When the seismic fractures coalesce into far-reaching pathways for fluid migration, the migrating fluid may reach pre-existing faults, and by decreasing fault strength, can trigger major seismic events. We assume that the potential for building such pathways depends on closeness of hypocenters, similarity of fracture planes orientations, and closeness of radii taking off from the injection point, on which events locate. We define this potential as the average distance between seismic events in the space of parameters quantifying the above conditions. We show that in the studied case from The Geysers geothermal field, this potential is highly correlated with injection rate. When the overall level of injection rate is high, the higher the injection rate, the more the potential for building far-reaching pathways for fluid migration is reduced.
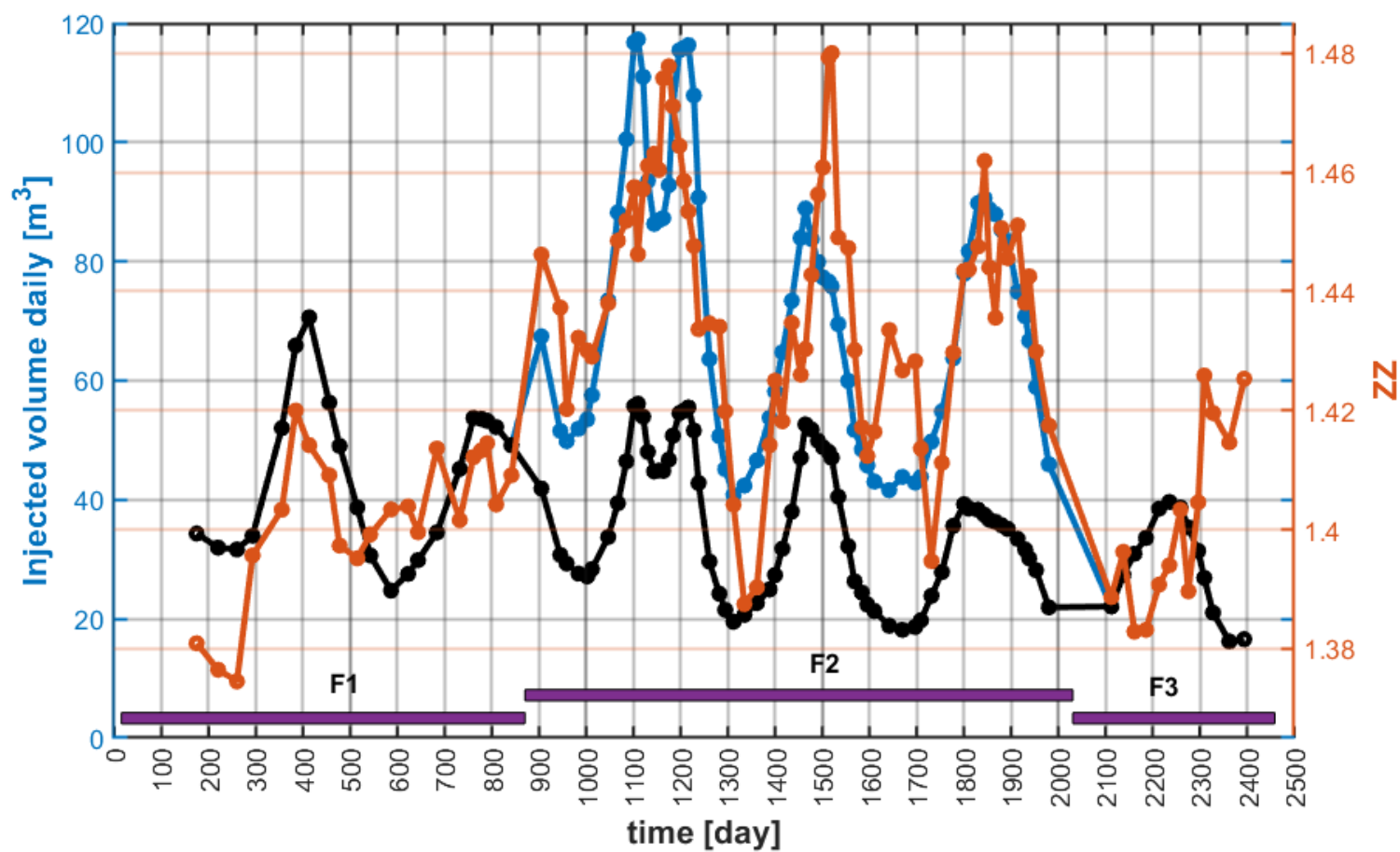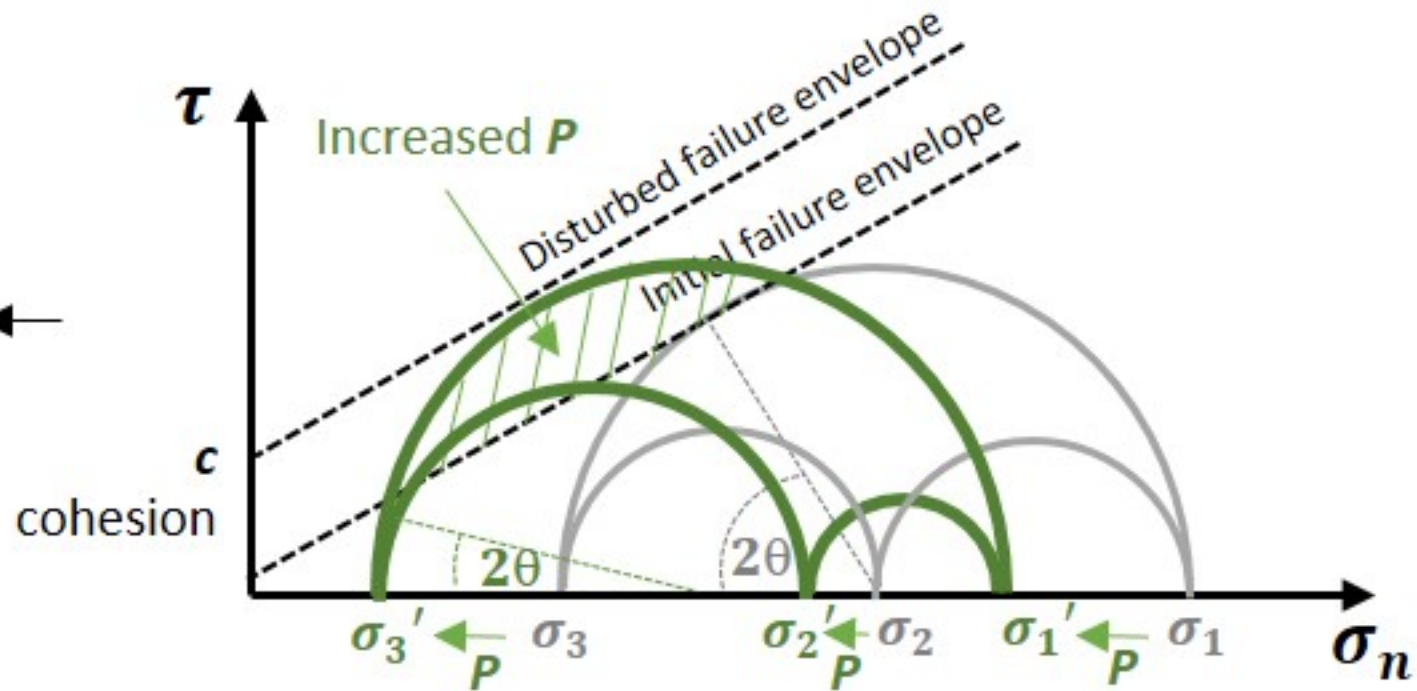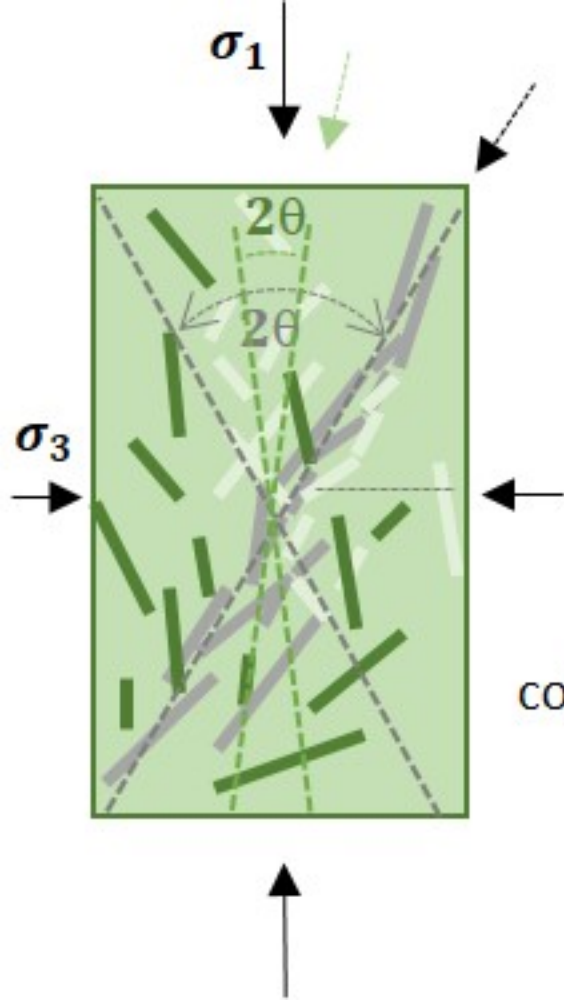
Figure 1.

Figure 2.

1
2
High injection rates counteract formation of far-reaching fluid migration pathways at The Geysers geothermal field

3

4
Stanisław Lasocki [1], and Beata Orlecka-Sikora [1]

5
[1]Institute of Geophysics Polish Academy of Sciences.

6
Corresponding author: Stanisław Lasocki (lasocki@igf.edu.pl)

7
Key Points:

8
9
- Degree of seismic sources disorder correlates with injection rate and amplitudes of its changes agree with injection rate changes.

10
11
- Formation of long pathways for fluid migration requires certain ordering of seismic sources.

12
13
- High injection rates increase sources disorder hence decrease chance for seismic fractures to coalesce into long fluid migration pathways.

14

15 **Abstract**

16 Deep underground water injections induce seismicity. When the seismic fractures coalesce into
17 far-reaching pathways for fluid migration, the migrating fluid may reach pre-existing faults, and
18 by decreasing fault strength, can trigger major seismic events. We assume that the potential for
19 building such pathways depends on closeness of hypocenters, similarity of fracture planes
20 orientations, and closeness of radii taking off from the injection point, on which events locate.
21 We define this potential as the average distance between seismic events in the space of
22 parameters quantifying the above conditions. We show that in the studied case from The Geysers
23 geothermal field, this potential is highly correlated with injection rate. When the overall level of
24 injection rate is high, the higher the injection rate, the more the potential for building far-
25 reaching pathways for fluid migration is reduced.

26 **Plain Language Summary**

27 Geothermal energy production is often based on pumping cold water down to hot rocks and
28 taking back steam. Pressurized underground water injections induce brittle fracturing of rocks,
29 that is seismic events, what enhances the rock permeability and in this way increases the surface
30 on which heat exchange takes place. However, the seismic fractures may also coalesce into
31 undesired pathways enabling the fluids to migrate far and reach pre-existing tectonically
32 preloaded faults. Then the fluids decrease fault strength, and in result the fault can rupture
33 producing a major seismic event. We studied how some properties of the seismicity induced by
34 injections of water in a part of the Geysers, which can lead to the mentioned undesired fracture
35 network development, depend on injection rates. Our studies indicated that the potential for such
36 network development is highly correlated with the injection rate. Moreover, it turned out that in
37 order to avoid this unwanted development of fracture network the injection rates should be kept
38 high. The higher the injection rate is, the more the potential for building far-reaching pathways
39 for fluid migration is reduced. These results, when confirmed on other seismically active
40 geothermal energy production cases can have important implications for strategies of
41 geothermics.

42 **1 Introduction**

43   Deep underground water injections induce seismicity. This seismic fracturing of rocks is
44 desirable as it increases the surface on which heat exchange takes place in Enhanced Geothermal
45 Systems. However, the seismic fractures may also coalesce into undesired pathways for fluid
46 migration. These are such pathways that enable the fluids to reach pre-existing faults. In result,
47 by decreasing fault strength, the fluids can trigger ruptures and produce major seismic events.
48 The further the migration pathways extend from the injection point, the more probable are these
49 unwanted effects. It is therefore of paramount importance to recognize under which injection
50 conditions an induced seismic process can produce such pathways (e.g.: Davies et al., 2013;
51 Ellsworth, 2013; Majer et al., 2012; Zhang Dongxiao & Yang Tingyun, 2015).

52   Numerous studies indicate that the geometry of fractures and the structure of fracture
53 networks are the main factors controlling fluid flow and the fluid transport characteristics of
54 rocks (e.g.: Hope et al., 2015; Lee et al., 1990; Long & Billaus, 1987; Schwartz et al., 1983;
55 Snow, 1965). The development of the fracturing process has been investigated in a number of
56 laboratory experiments (e.g.: Ko & Kemeny, 2011; Lockner et al., 1992; Stanchits et al., 2006).
57 Based on these experiments, many models have been developed to simulate the geometry of

58   fractures and the topology of fracture networks (e.g.: Hope et al., 2015; Lee et al., 1990; Long &
59   Billaus, 1987). However, although seismic field data provide direct insight into the development
60   of fracture networks at the crustal scale, there are few studies focused on this topic (e.g.:
61   Chorozoglou et al., 2018; Kagan,1992; 2000; Orlecka-Sikora et al., 2019; Sausse et al., 2010).

62   Here we study seismic and injection data from a part of the Geysers geothermal field to
63   determine a relationship between the injection conditions and the potential of injection-induced
64   seismicity to build far-reaching pathways for fluid migration. We formulate three conditions
65   which we expect to play a role in linking fractures and building such pathways: closeness of
66   hypocenters; similarity of fracture planes orientations; closeness of radii, which begin at the open
67   hole section of the injection well and on which events occur. We assume that in the same
68   injection conditions and for the same orientation of the line connecting hypocenters of two
69   events with respect to the orientation of regional stress field, the probability for these events to
70   link is higher when they are closer to each other than when they are farther from each other. We
71   assume that, for the same stress and injection conditions and the same distance between
72   hypocenters, when the fault planes of two events are parallel and they are parallel to the line
73   connecting hypocenters, the probability for these events to link is higher than this probability for
74   other mutual orientations of fault planes. Moreover, when they have linked they more likely
75   extend farther than the linked fractures with other fault plane orientations. We assume that linked
76   fractures located along the straight line beginning at the injection point reach farther from this
77   point than such fractures located in another way.

78   Consequently, seismic events are represented by eight parameters: three hypocentral
79   coordinates, three independent angles determining orientations of the T and P axes of the double-
80   couple focal mechanisms, and two angular coordinates of hypocenters in the spherical system
81   beginning at the open hole of injection well. To achieve the same scaling of these parameters, we
82   transform them to equivalent dimensions (ED) (Lasocki, 2014; Supporting Information Text S1).
83   The average distance between the events in the 8-dimensional space of the aforementioned
84   parameters, called the degree of disordering of sources, *ZZ*, expresses to which extent the above
85   three conditions have been fulfilled. The chance for the seismic events with small value of *ZZ*,
86   that they link and reach far is higher than in other cases. In this way ZZ quantifies the potential
87   for building far-reaching fluid migration pathways.

88   We show that *ZZ* is highly significantly correlated with injection rate. *ZZ* took the highest
89   values when the injection rates were the highest, which indicates that high injection rates
90   counteracted the formation of far-reaching fluid migration pathways.

91 **2 Data and Methods**

92   The Geysers geothermal field is located in California, US. Geothermal operations, which
93   began there in 1960s, and which presently use EGS technology, have induced hundreds of
94   thousands of seismic events. We studied injection and seismic data from an isolated area of 2 km
95   × 2 km in the NW part of The Geysers, between 10 December 2007 and 23 August 2014. The
96   basis for the seismic dataset was an improved catalog that contained 1252 events (Kwiatek et al.,
97   2015; Martínez-Garzón et al., 2014; 2016). This catalog provided all the event parameters,
98   necessary for the calculation of the degree of disordering of sources, *ZZ*: hypocenter locations
99   with an accuracy of 50 m, and focal mechanisms with an accuracy of 20°/5°/10° for
100 strike/dip/rake. The focal mechanisms were used to recover the trend and plunge angles of T and
101 P axes. Moment magnitude was used and the completeness level was Mc=1.4 (Kwiatek et al.,

102 2015). The strongest event was Mw3.2. Hypocenter locations and magnitude distributions are
103 provided in Supporting Information Figures S1-S5.

104   In the study period, the injections in the study area were carried out into two wells: Prati9
105 and Prati29. There were three phases of the injection activity:

106   • Phase F1 from 10 December 2007 to 10 April 2010, in which only Prati9 was
107   operational,
108   • Phase F2 from 11 April 2010 to 21 June 2013 with simultaneous injections into both
109   wells,
110   • Phase F3 from 11 June 2013 to the end of the study period, in which only Prati9 was
111   operational.

112   The injection data consisted of the daily injection volumes into Prati9 and Prati29.

113   Most of the 1252 seismic events clustered around the open hole of Prati9 well (see:
114 Supporting Information Figures S1-S4). We intended to analyze the relationship between
115 injection and the degree of disordering of sources, *ZZ*, within the whole time period of available
116 data, in which period only Prati9 well was constantly operational. Therefore we studied these
117 events located closer to Prati9 well, expecting that their spatial relation to Prati9 resulted from
118 their physical relation to the injection activity in Prati9. As the selection criterion we used the
119 hypocentral distance from the open hole of Prati9 to be no more than 600 m. 1121 events that
120 fulfilled this criterion are called cluster A.

121   The degree of disordering of sources, *ZZ*, used to quantify the potential for building the
122 far-reaching fluid migration pathways, was the average distance between the seismic events in
123 the 8-dimensional parameter space {x_1, x_2, x_3, *plu_X_1*, *plu_X_2*, *tre_X_1*, Θ, φ}. $x_{1,2,3}$ were
124 hypocenter coordinates. *plu_X_1* , *tre_X_1* were the plunge and trend angles of T axis. *plu_X_2* was
125 the plunge angle of P axis. Θ, φ were the polar and azimuthal angles of hypocenter in the
126 spherical system of coordinates beginning at the open hole of Prati9 well. Θ=0 for the vertical
127 direction and φ=0 for the N direction. These parameters were not comparable therefore we first
128 transformed them to ED. The transformation to ED is a technique based on a probabilistic
129 equivalence of the parameters that scale differently (Lasocki, 2014; Supporting Information Text
130 S1). All transformed parameters are uniformly distributed in [0,1] and the distance between any
131 two objects is the Euclidean metric. Further on the symbols x_1, x_2, x_3, *tre_X_1*, *tre_X_2*, *plu_X_1*,
132 *plu_X_2*, Θ, φ denote the EDs of the original source parameters.

133   The closeness of hypocenters was parameterized by the absolute differences between
134 hypocenter coordinates, $\Delta x_k(i,j) = |x_k(i) - x_k(j)|, k = 1,2,3$.

135   The trend angle and the polar angle take values in [0°, 180°], which is [0, 1] in ED, and
136 the azimuthal angle takes values in [0°, 360°], which is also [0,1] in ED. The shortest distances
137 between these angles in ED were therefore:

138 $$\Delta tre\_X_1(i,j) = 2 \begin{cases} |tre\_X_1(i) - tre\_X_1(j)| & if \ |tre\_X_1(i) - tre\_X_1(j)| \leq 0.5 \\ 1 - |tre\_X_1(i) - tre\_X_1(j)| & if \ |tre\_X_1(i) - tre\_X_1(j)| > 0.5 \end{cases}, \quad (1)$$

139 $$\Delta\theta(i,j) = 2 \begin{cases} |\theta_i - \theta_j| & if \ |\theta_i - \theta_j| \leq 0.5 \\ 1 - |\theta_i - \theta_j| & if \ |\theta_i - \theta_j| > 0.5 \end{cases}, \quad (2)$$

140
$$\Delta\varphi(i,j) = 4 \begin{cases} |\varphi(i) - \varphi(j)| & if \ \ |\varphi(i) - \varphi(j)| \leq 0.25 \\ |0.5 - |\varphi(i) - \varphi(j)|| & if \ \ 0.25 < |\varphi(i) - \varphi(j)| \leq 0.75 \\ 1 - |\varphi(i) - \varphi(j)| & if \ \ |\varphi(i) - \varphi(j)| > 0.75 \end{cases} . \tag{3}$$

141   The multipliers in front of the opening braces in equations (1-3) were inserted so that the
142 differences in all parameters scaled in [0, 1].

143   The plunge angle takes values in [0°, 90°], hence, $\Delta plu\_X_k(i,j)$ was always $|plu\_X_k(i) -$
144 $plu\_X_k(j)|$, k=1,2.

145   For a collection of n seismic sources the degree of disordering of sources, ZZ reads:

146
$$ZZ = \left\{ \sum_{i=1}^{n-1} \sum_{j=i+1}^{n} ZZ(i,j) \right\} / \frac{n(n-1)}{2} \tag{4}$$

147   where

148        $ZZ(i,j) =$

149 $\sqrt{[\sum_{k=1}^{3} \Delta x_k(i,j)^2] + [\Delta tre\_X_1(i,j)^2 + \sum_{k=1}^{2} \Delta plu\_X_k(i,j)^2] + [\Delta\theta(i,j)^2 + \Delta\varphi(i,j)^2]} =$

150 $\sqrt{\Delta_r(i,j)^2 + \Delta_M(i,j)^2 + \Delta_\phi(i,j)^2}$ (4a)

151        $\Delta_r(i,j)$ is the distance between hypocenters of events i and j;

152        $\Delta_M(i,j)$ is the distance between focal mechanisms of these two events;

153        $\Delta_\phi(i,j)$ is the distance between the directions of radii from the Prati9 open hole, those on
154 which the hypocenters of these two events locate.

155   We carried out our analyses separately in the three injections phases. Out of 1121 studied
156 events, 248 events occurred in the injection phase F1, 702 events – in phase F2 and 171 events –
157 in phase F3. For every injection phase we calculated ZZ for 50-event window sliding by 10
158 events because the number of events per phase was not high enough to use non-overlapping
159 windows. We obtained 21 ZZ values for F1, 66 ZZ values for F2 and 13 ZZ values for F3.

160   Next, we calculated the average injection rates, *IN*, during time windows covering the
161 periods of the 50-event sliding windows, respectively. The calculations were performed for the
162 injection rate periods exactly matching the periods of respective 50-event windows and for the
163 injection rate periods from 1 to 21 days preceding the periods of event windows. The latter part
164 of this analysis was meant to study delayed reactions of seismicity.

165   Finally, we studied the correlation between ZZ and *IN*. It comes from equation (4a) that
166 ZZ is composed of three components representing our three conditions determining the potential
167 of injection-induced seismicity for building far-reaching pathways for fluid migration. In order to
168 recognize contributions of these components to the correlations between ZZ and *IN* we studied
169 also the correlations between Δ_r, Δ_M, Δ_ϕ and *IN*, respectively.

170   All correlation analyses were preceded by the Jarque-Bera test applied to check normality
171 of the distributions of used variables. If the normality hypothesis was not rejected we used
172 Pearson correlation, otherwise we used Spearman correlation.

173   We also tested differences between the values of location parameters by phase of *IN*, *ZZ*,
174 seismic activity rate and magnitude, respectively. When the normality hypothesis for a parameter

175   was not rejected, we used the Student's t-test for means, otherwise we applied the Mann-
176   Whitney U-test for medians. All statistical inferences were performed under the significance
177   level α=0.05.

3 Results and Discussion

179   Some descriptive statistics by injection phase of *IN*, *ZZ*, seismic activity rate and
180   magnitude of events are presented in Table 1 together with comparisons of their location
181   parameters (means or medians) among phases. The medians of injection rates into Prati9 well
182   were decreasing statistically significantly with injection phase.

183   Figure 1 compares the time-variations of *ZZ*, with the variations of average injection rate,
184   *IN*. In phase F2 this comparison concerns the injection rate into Prati9 well, *IN*(9), and the total
185   injection rate into both wells, *IN*(both). It is seen that in the first two injection phases, F1 and F2,
186   *ZZ* correlated positively with *IN*. Also the amplitudes of the *ZZ*-changes agreed well with the
187   amplitudes of the average injection rate changes. In phase F2, this agreement related to the
188   summed injection into both wells (blue curve) rather than into Prati9 well alone (black curve),
189   even though the analyzed seismic events were geometrically linked to Prati9 (Supporting
190   Information Figures S1-S4).

191   Table 2 presents the results of analysis of correlations between the injection rate, *IN*, and
192   *ZZ*. For all average injection rate series and for most *ZZ* and its components' series the normality
193   hypothesis was not rejected. For these cases the analysis was based on Pearson's linear
194   correlation coefficient. The exceptional cases were correlations with Δ_ϕ in phase F2 because Δ_ϕ
195   series in this phase was not normally distributed. In these two cases Spearman's rank correlation
196   was used.

197   The results in Table 2 confirm the relationships evidenced in Figure 1. In F1 and F2 the
198   correlation between *IN* and *ZZ* was significant, positive. In F2 this correlation was highly
199   significant, irrespective of whether the *IN* referred to injections into Prati9 or to the summed
200   injections into Prati9 and Prati29 wells. The *ZZ* vs. *IN*(9) scatterplot is presented in Supporting
201   Information Figure S6.

202   The results of correlation analysis for delayed *ZZ* with respect to *IN* are presented in
203   Supporting Information Tables S1-S4. In F1 the correlation coefficient slowly decreases with
204   increasing lag. The correlation coefficient in F2 slightly increased when *ZZ* was delayed with
205   respect to *IN*, however the difference between the correlation coefficient for zero lag and for 13
206   days lag was only 0.022 and was surely insignificant.

207   The previous studies of the same data have indicated a positive correlation between
208   seismicity rates and injection rates (Leptokaropoulos et al., 2018). Hence different time periods
209   corresponded here to the 50-events windows; the time periods at higher injection rates were
210   shorter. We checked whether the positive *ZZ* vs. *IN* correlations were not due to these differences
211   between time periods. We divided phase F2 into non-overlapping windows of constant, 68 days
212   duration. The correlation between *IN* and *ZZ* both calculated for these windows of constant time
213   period, was also positive (0.87) and significant ($p = 0.0097$).

214   In F1 only Δ_r out of three components of *ZZ* significantly and positively correlated with
215 *IN*. Hence, in this injection phase the positive *ZZ* - *IN* correlation resulted from that that higher
216 injection rates were increasing distances between the sources.

217   In F2 all three distances, $\Delta_r, \Delta_M, \Delta_\phi$, were highly positively correlated with *IN* thus they
218 all significantly contributed to the correlation *ZZ* – *IN*. Higher injection rates led to an increase of
219 the distances between hypocenters, to a greater variety of P and T axes directions and to a greater
220 angular dispersion of the hypocenters in relation to the open hole of Prati9 well.

221   The significant correlation Δ_r – *IN* in F1 and F2 cannot be attributed just to moving away
222 sources from the well opening of Prati9 when the injection rates were higher. The correlation
223 between the average distance from the Prati9 opening and *IN* was significant in F1 (corr.
224 coefficient 0.47, $p=0.03$), though much weaker that the Δ_r – *IN* correlation, and in F2 it was
225 insignificant (corr. coefficient 0.14, $p=0.28$).

226   Our target was studying the relationship between the degree of disordering of seismic
227 sources, *ZZ*, and the injection rate, *IN*. We used the transformation to ED because the
228 components of *ZZ*: the distances between *P* (and *T*) axes of events and the distances between
229 radii on which events located, are not Euclidean. However, the metrics of the distance between
230 hypocenter locations is Euclidean. Thus, it was possible to compare the shown here results of
231 correlation between Δ_r and *IN* in F1 and F2, based on the transformation to ED, with such results
232 based on more often used inter-event distance analyses. As alternatives to Δ_r we used correlation
233 dimension of distances between hypocenters, D_2, and summarized squared distances in the
234 original (x,y,z) space, $d2$. D_2 turned out to be uncorrelated with *IN*, probably because difficulties
235 with its estimation. The correlation between $d2$ and *IN* was even stronger than between Δ_r and
236 *IN*. We think that this was due to the fact that any transformation, here the transformation to ED
237 causes some loss of information. Nevertheless, the same significant correlation between $d2$ and
238 *IN* as the correlation between Δ_r and *IN* positively validated the performance of transformation
239 to ED. The results of this part of analysis are provided and discussed in Supporting Information
240 Text S2.

241   The significant impact of fluids on the stress field and the faulting regime is known from
242 many studies (e.g., Segall and Fitzgerald,1998; Hardebeck and Hauksson, 1999; Bachmann et
243 al., 2012). The analyses of seismic events from the NW part of The Geysers geothermal field,
244 presented in Martínez-Garzón et al. (2013, 2016) and Kwiatek et al. (2015), clearly show a large
245 variability of focal mechanisms. Explaining the observed stress tensor perturbation the cited
246 authors consider the fact that in addition to fracture reactivation, massive fluid injection in EGS
247 systems results in hydro-fracturing. It is then possible that during the time periods of higher
248 injection rates, new small fractures were created and they could also perturb the stress field in the
249 observed way (Martínez-Garzón et al., 2016). A number of events occurred either on severely
250 misoriented faults (low instability coefficient, eg. Vavryčuk, 2011) or slipped in a different
251 orientation than the predicted from the stress field. These events mostly occurred during periods
252 of high injection rates indicating that faults not optimally oriented to the stress field require
253 larger pore pressures to become activated.

254   A way in which increased injection rates may increase the degree of disordering of
255 sources (*ZZ*) is shown schematically in Figure 2. An increase of pore pressure resulting from the
256 increased injection rate broadens the range of possible orientations and locations for new shear
257 fractures.

258   Studying fracture network development on the same data as here, Orlecka-Sikora et al.
259   (2019) have shown that the connectivity of fractures induced by fluid injection is lower for
260   higher injection rates and *vice versa*. Thus the connectivity was responding to the injection rate
261   changes in the same way as *ZZ*. This allows for inferring that *ZZ* indeed represents the potential
262   for fluid migration. In the cited work the connectivity was estimated by the connectivity
263   coefficient, *C*, defined by the ratio of the observed number of intersections of fractures in a
264   fracture network to the number of all possible intersections in this network. These all possible
265   intersections were evaluated as $0.5f(f-1)$, where f was the number of fractures building the
266   fracture network (Albert & Barabasi, 2002; Watts & Strogatz, 1998).

267   Prati29 well was operational only in phase F2. In this phase the amplitudes of *ZZ* changes
268   agreed with the amplitudes of changes of the summarized injections into Prati9 and Prati29.
269   Furthermore, the mean level of *ZZ* and the mean seismic activity were the highest in this phase
270   and significantly higher than in phases F1 and F3. In F2 only the level of total injection into
271   Prati9 and Prati29 was the highest, and the mean level of injection rate into the Prati9 well was
272   significantly smaller than in phase F1. All these indicate the important role of the injections into
273   Prati29 for the generation of seismic events within the studied cluster A despite the Prati29 well
274   location being outside cluster A.

275   The seismic events generated at higher injection rates, i.e. the ones more disordered (*ZZ*
276   was higher), did not have greater magnitudes. On the contrary, in phase F1 the mean magnitude
277   in windows correlated negatively with *ZZ* (corr. coef. -0.61, $p = 0.003$). In F2 no magnitude – *ZZ*
278   correlation was ascertained.

279   In phase F3, in which the overall level of injection rate was the lowest among injection
280   phases, the correlation *IN - ZZ*, was significant, negative. This correlation was achieved only
281   jointly by the three components of *ZZ*: $\Delta_r, \Delta_M, \Delta_\phi$ because neither of them significantly
282   correlated with *IN*. The negative correlation coefficient in F3 increased when *ZZ* was delayed
283   with respect to *IN*, and for 4 and more days lag it became statistically not significant (Supporting
284   Information Table S4). This reversal of correlation results may be connected with another
285   fracture mechanism below a certain level of injection rate. We discuss this possibility in
286   Supporting Information Text S3. However, the data series in F3 was composed of only 13 points
287   therefore the correlation (p≈0.03) might be spurious.

288 4 Conclusions

289   Studying the actual field data we found exceptionally high and immediate correlation
290   between the injection rate and the seismicity parameter - the degree of disordering of sources,
291   *ZZ*. Also the amplitudes of *ZZ*-changes agreed well with the amplitudes of average injection rate
292   changes. *ZZ* is defined solely on parameters of seismic sources. It describes how much seismic
293   fractures are dispersed in terms of distances between their hypocenters, mutual orientations of
294   their fracture planes, and angular dispersion of their hypocenters. In the next work we will
295   modify *ZZ* to account also for source sizes.

296   We interpret *ZZ* as a measure of the potential of seismic fractures for building far-
297   reaching pathways for fluid migration. The logic of the three conditions, on which *ZZ* is based,
298   supports this interpretation. However, ZZ does not represent all possibilities for building such a
299   fracture system neither it is adequate for other possibilities of fracture network development (e.g.
300   not for a percolating fluid pathway).

301   In the studied case from The Geysers geothermal field, the optimal conditions to avoid
302 such ordering of seismic fractures that enable linking them into longer pathways, extending
303 farther from the injection point were met for high injection rates. The higher the injection rate
304 was, the more disordered the seismic fractures were generated, i.e., the chances to build longer
305 pathways for undesired fluid migration decreased. High injection rates caused an increase in
306 seismic activity, nevertheless the median level of seismic event magnitudes remained unaffected.

307   The above conclusion, if confirmed in other cases of injection induced seismicity, would
308 help to understand this type of seismicity and related hazards. Martínez-Garzón, et al. (2018)
309 conclude that the used here dataset from the NW region of The Geysers well represents the
310 broader seismic processes at The Geysers field. Thus our results may be also valid for all seismic
311 processes at The Geysers. However, for further generalizations studies of other injection-induced
312 seismicity cases are required.

Acknowledgments

323

References:

Albert, R. & Barabasi, A.L. (2002) Statistical mechanics of complex network, *Reviews of Modern Physics*, 74, 47–97.

Bachmann, C.E., Wiemer, S., Goertz-Allmann, B.P. & Woessner, J. (2012) Influence of pore-pressure on the event-size distribution of induced earthquakes, *Geophysical Research Letters*, 39, L09302, doi:10.1029/2012GL051480

Chorozoglou, D., Kugiumtzis, D., & Papadimitriou, E. (2018) Testing the structure of earthquake networks from multivariate time series of successive main shocks in Greece, *Physica A*, 499, 28–39.

Davies, R., Foulger, G., Bindley, A., & Styles, P. (2013) Induced seismicity and hydraulic fracturing for the recovery of hydrocarbons, *Marine and Petroleum Geology*, 45, 171-185.

Ellsworth, W.L. (2013) Injection-induced earthquakes, *Science*, 341, 6142, doi: 10.1126/science.1225942

Hardebeck, J.L. & Hauksson, E. (1999) Role of fluids in faulting inferred from stress field signatures. *Science* 285 (5425), 236-239, DOI: 10.1126/science.285.5425.236

Hope, S.M., Davy, P., Maillot, J., Le Goc, R., & Hansen, A. (2015) Topological impact of constrained fracture growth. *Frontiers in Physics* 3-75.

Kagan, Y.Y. (1992) Correlations of earthquake focal mechanisms. *Geophysical Journal International*, 110, 305-320.

Kagan, Y.Y. (2000) Temporal correlations of earthquake focal mechanisms. *Geophysical Journal International*, 143, 881-897.

Ko, T.Y., & Kemeny, J. (2011) Subcritical crack growth in rocks under shear loading. *Journal of Geophysical Research*, *Solid Earth*, 116, B01407, doi:10.1029/2010JB0008461.

Kwiatek, G., Martínez-Garzón, P., Dresen, G., Bohnhoff, M., Sone, H., & Hartline, C. (2015) Effects of long-term fluid injection on induced seismicity parameters and maximum magnitude in northwestern part of The Geysers geothermal field. *Journal of Geophysical Research*, *Solid Earth*, 120, 7085–7101, doi: 10.1002/2015JB012362.

Lasocki, S. (2014) Transformation to equivalent dimensions – a new methodology to study earthquake clustering. *Geophysical Journal International*, 197 (2), 1224-1235.

Lee, J.S., Veneziano, D., & Einstein, H.H. (1990) "Hierarchical fracture trace model" In Rock Mechanics Contributions and Challenges: Proceedings of the 31st US Symposium on Rock Mechanics, W. Hustrulid, W., & Johnson, G.A., Eds. (A.A. Balkema 1990), pp. 261-268.

Leptokaropoulos, K., Staszek, M., Lasocki, S., Martínez-Garzón, P., & Kwiatek, G. (2018) Evolution of seismicity in relation to fluid injection in the North-Western part of The Geysers geothermal field. *Geophysical Journal International*, 212, 1157–1166, doi: 10.1093/gji/ggx481

Lockner, D.A., Byerlee, J., Kuksenko, V., Ponomarev, A., & Sidorin, A. (1992) "Observations of quasi-static fault growth and acoustic emissions" in Fault Mechanics and Transport Properties of Rocks, B. Evans and T.-F. Wong, Eds. (Academic, London 1992), pp. 3–31.

Long, J.C.S., & Billaus, D.M. (1987) From field data to fracture network modeling: An example incorporating special structure, *Water Resources Research*, 23(7), 1201-1216.

Majer, E., Nelson, J., Robertson-Tait, A., Savy, J., & Wong, I. (2012) Protocol for Addressing Induced Seismicity Associated with Enhanced Geothermal Systems, *Geothermal Technologies Program U.S. Department of Energy, Energy Efficiency & Renewable Energy*

Martínez-Garzón, P., Bohnhoff, M., Kwiatek, G. & Dresen, G. (2013) Stress tensor changes related to fluid injection at The Geysers geothermal field, California, *Geophysical Research Letters*, 40, 2596–2601, doi:10.1002/grl.50438

370   Martínez-Garzón, P., Kwiatek, G., Sone, H., Bohnhoff, M., Dresen, G., & Hartline, C. (2014)
371   Spatiotemporal changes, faulting regimes, and source parameters of induced seismicity: A case
372   study from The Geysers geothermal field. *Journal of Geophysical Research. Solid Earth*, 119,
373   8378–8396, doi: 10.1002/2014JB011385.
374   Martínez-Garzón, P., Kwiatek, G., Bohnhoff, M., & Dresen, G. (2016) Impact of fluid injection
375   on fracture reactivation at The Geysers geothermal field, *Journal of Geophysical Research. Solid*
376   *Earth*, 121(10), 7432–7449, doi: 10.1002/2016JB013137.
377   Martínez-Garzón, P., Zaliapin, I., Ben-Zion, Y., Kwiatek, G. & Bohnhoff, M. (2018)
378   Comparative study of earthquake clustering in relation to hydraulic activities at geothermal fields
379   in California. *Journal of Geophysical Research. Solid Earth*, 123, 4041–4062,
380   https://doi.org/10.1029/2017JB014972.
381   Orlecka-Sikora, B., Cielesta, S., & Lasocki, S. (2019) Tracking the development of seismic
382   fracture network from The Geysers geothermal field. *Acta Geophysica*, 67, 341-350.
383   Sausse, J.C., Dezayes, C., Dorbath, L. Genter, A., & Place, J. (2010) 3D model of fracture zones
384   at Soultz-sous-Forêts based on geological data, image logs, induced microseismicity and vertical
385   seismic profiles. *Comptes Rendus Geo-sciences*, 342(7-8), 531-545.
386   Schwartz, F.W., Smith, L. & Crowe, A.S. (1983) A stochastic analysis of macroscopic dispersion
387   in fractured media, *Water Resources Research*, 19(5), 1253-1265.
388   Segall, P. & Fitzgerald, S.D. (1998) A note on induced stress changes in hydrocarbon and
389   geothermal reservoirs. *Tectonophysics*, 289, 117–128.
390   Snow, D.T. (1965) A parallel plate model fractured permeable media, PhD. Thesis, Univ. of
391   Calif., Berkeley.
392   Stanchits, S., Dresen, G., & Guéguen, Y. (2006) Ultrasonic velocities, acoustic emission
393   characteristics and crack damage of basalt and granite, *Pure Applied Geophysics*, 163(5–6), 975–
394   994.
395   Vavryčuk, V. (2011) Principal earthquakes: theory and observations from the 2008 West
396   Bohemia swarm, *Earth and Planetary Science Letters*, 305, 290–296, doi:
397   10.1016/j.epsl.2011.03.002.
398   Warren-Smith, E., Fry, B., Wallace, L., Chon, E., Henrys, S., Sheehan, A., Mochizuki, K.,
399   Schwartz, S., Webb, S. & Lebedev, S. (2019) Episodic stress and fluid pressure cycling in
400   subducting oceanic crust during slow slip. *Nature Geoscience*, 12, 475–481,
401   doi.org/10.1038/s41561-019-0367-x.
402   Watts, D.J. & Strogatz, S.H. (1998) Collective dynamics od "small-world" networks, *Nature*,
403   393, 440–442.
404   Zhang Dongxiao & Yang Tingyun (2015) Environmental impacts of hydraulic fracturing in shale
405   gas development in the United States, *Petroleum Exploration and Development*, 42(6), 876–883.
406
407

408 **Tables:**

409 **Table 1.** Descriptive statistics and comparisons of the average injection rate, *IN*, the degree of
410 disordering of seismic sources, ZZ, the activity rate, and magnitude of events in the three
411 injection phases. The magnitude was transformed to the equivalent dimension. The other
412 quantities: *IN* and activity rate were not. The column "Comparisons" contains *p*-values of the
413 tests of differences between means or medians of these parameters. The significant differences
414 are in bold.

	Injection phase									Comparisons of location parameters, *p*-value		
	F1			F2			F3			F1 vs. F2	F2 vs. F3	F1 vs. F3
	Mean	Med.	Std. dev.	Mean	Med.	Std. dev.	Mean	Med.	Std. dev.			
Prati9 *IN* [100m^3/day]	43.76	45.18	13.09	36.18	35.69	11.51	29.10	30.95	8.18	**0.024**	**0.014**	**3E-4**
Summed Prati9 and Prati29 *IN* [100m^3/day]	43.76	45.18	13.09	72.82	73.43	22.54	29.10	30.95	8.18	------------------------		
ZZ	1.402	1.403	0.012	1.439	1.438	0.021	1.401	1.396	0.015	**5E-14**	**2E-7**	0.91
Activity rate [event/day]	0.35	0.34	0.13	0.70	0.69	0.23	0.48	0.44	0.11	**7E-12**	**6E-6**	**7E-3**
Magnitude	0.55	0.57	0.06	0.49	0.49	0.04	0.45	0.47	0.06	**3E-4**	0.055	**2E-4**

415
416
417 **Table 2.** Results of the correlation analysis between the average injection rate, *IN*, and ZZ, and
418 its components, $\Delta_r, \Delta_M, \Delta_\phi$. For phase F2 row 'a' provides the correlation between *ZZ* and *IN*
419 into Prati9 well, and row 'b' provides the correlation between *ZZ* and total *IN* into Prati9 and
420 Prati29 wells. The significant correlations are in bold. The results based on Spearman rank
421 correlation are in italics.

Injection phase	ZZ		Δ_r		Δ_M		Δ_ϕ	
	Corr. coef.	*p*-value	Corr. coef.	*p*-value	Corr. coef.	*p*-value	Corr. coef.	*p*-value
F1	**0.62**	**0.002**	**0.69**	**5·10^{-4}**	0.20	0.37	-0.28	0.22
F2 – a	**0.76**	**2·10^{-13}**	**0.69**	**2·10^{-10}**	**0.41**	**7·10^{-4}**	*0.49*	*3·10^{-5}*
F2 – b	**0.72**	**7·10^{-12}**	**0.65**	**1·10^{-9}**	**0.45**	**1·10^{-4}**	*0.47*	*8·10^{-5}*
F3	**-0.60**	**0.029**	-0.20	0.51	-0.32	0.28	-0.19	0.52

422
423

424 **Figure captions:**
425
426   **Figure 1.** Comparison of the time-variation of *ZZ* with the time-changes of average
427   injection rate. Black – the injection rate into Prati9 well, blue – the total injection rate into
428   Prati9 and Prati29 wells, brown – *ZZ*. The horizontal bars mark the durations of injection
429   phases.

430   **Figure 2.** Schematic presentation of influence of pore pressure (P) changes on the failure
431   plane orientations. The linear failure criterion imposes that shear fractures make with σ_1 a
432   well-defined angle of ($\pm$) $45°-\varphi/2$, where φ is the angle of internal friction, and $\theta = \phi/2 + 45$
433   (gray circle in Coulomb-Mohr diagram and gray fractures on the rock block on the left).
434   An increase of P reduces the effective normal stress, σ_n', where $\sigma_n' = \sigma_n - P$ and broadens
435   the range of possible orientations for new shear fractures (all directions going through
436   green hatched area in the Coulomb-Mohr diagram and green fractures on the rock block)
437   (after Warren-Smith et al., 2019).

438

1

3   Supporting Information for

4   **High injection rates counteract formation of far-reaching fluid migration pathways at**
5   **The Geysers geothermal field**

6   Stanisław Lasocki[1], and Beata Orlecka-Sikora[1]

7   [1]Institute of Geophysics Polish Academy of Sciences

8

9

Contents of this file

11
22
23
24
25

Introduction

27 Text S1 presents briefly the transformation to equivalent dimension technique. This
28 transformation was applied to eight parameters that represented seismic events in
29 calculations of the degree of disordering of sources, *ZZ*. *ZZ* was determined by distances
30 between the events seen as points in 8D space of these parameters. *ZZ* could not be evaluated
31 from original values of these parameters because these parameters were not comparable and
32 five of them did not have the Euclidean metric. The transformation to equivalent dimensions
33 is suited for such problems. After transformation any set of parameters becomes comparable
34 and the parameter space metric becomes Euclidean. The text S1 presents the problem,
35 provides the assumptions of the transformation, defines equivalent dimensions, presents their

36   properties and the algorithm of the transformation. The address of the web page from where
37   the MATLAB codes of the transformation can be downloaded is also provided.

38   Figures S1 to S4 present the locations of hypocenters of the analyzed seismic events in the 3D
39   view and in the three 2D projections. The events marked by blue circles indicate locations of
40   the event from the cluster A, which have been analyzed in this paper. The other events from
41   the initial dataset are marked by black squares. The size of markers is proportional to the
42   magnitude of events. Locations of the open holes of the injection wells Prati9 and Prati29 are
43   also provided.

44   Figures S5 presents magnitude distribution of all events as well as of the events from
45   particular injection phases.

46   Figure S6 presents the scatterplots of the degree of disordering of sources, ZZ vs. the average
47   injection rate into Prati9 well, IN(9), in the injection phases F1 and F2.

48   Tables S1-S4 compliment Table 2 and present the results of the correlation analysis between
49   the injection rate, IN, and the degree of disordering of sources, ZZ and the three components
50   of ZZ for the ZZ and its components delayed with respect to IN values from zero to 21 days,
51   step one day. Table S1 contains the results for the injection phase F1, Tables S2 and S3 contain
52   the results for the injection phase F2 and Table S4 contains the results for the injection phase
53   F3. The results in Table S2 relate to the correlations with the injections into the injection well
54   Prati9 and the results in Table S3 relate to the correlations with the summed injections into
55   Prati9 and Prati29 wells.

56   Text S2 compares the results of correlation analysis between injection rate and three different
57   representations of closeness of hypocenters namely: (1) the average distance between
58   hypocenters in equivalent dimension space, Δ_r – the parameter used in the main text, (2) the
59   correlation dimension of distance between hypocenters, (3) the summarized squared distance
60   between hypocenters in original Cartesian system of coordinates. The comparison has been
61   performed on the data from phase F1.

62   In Text S3 we present a possible explanation of the obtained in phase F3 anticorrelation
63   between the degree of disordering of sources, ZZ, and the injection rate.

64

Text S1. Summary of the transformation to equivalent dimension technique (Lasocki, 2014)

Parameters of Seismic Events

- Source parameters: *t, lat, lon, depth, M, [$M_{i,j}$], E_s,* $\Delta\sigma$, r_0 etc.
- Derived from source parameters of two or more events e.g.: interevent time - τ, distance between this and the main shock - *r*, etc.
- Other having unambiguous association with seismic events e.g.
  - Parameters of the environment in which the event occurs: e_1, e_2, e_3
  - Parameters of inducing technological activity for anthropogenic seismicity: l_1, l_2, l_3 ...
  - ………………………………

A seismic event ≡ A point in a parameter space e.g. : **X**= [*t, lat, lon, depth, M, [$M_{i,j}$], E_s* $\Delta\sigma$, r_0, …, τ, r, …, e_1, e_2, e_3, ..., l_1, l_2, l_3, ..., ...]

Problem: Parameters of seismic events are not comparable and may have non-Euclidean metric.

Equivalent dimensions – Assumptions:
- Let seismic events be represented by the set of parameters X_k, k=1,..,p,. The population of these events is fully characterized by the probabilistic distributions of the parameters $F(X_k)$, k=1,..,p.
- Two intervals of the parameter values, [$x_{k,i},x_{k,j}$] , [$x_{l,s},x_{l,t}$] are equivalent if Prob($X_k\in$ [$x_{k,i},x_{k,j}$]) = Prob($X_l\in$ [$x_{l,s},x_{l,t}$]).
- The parameters X_k, k=1,..,p, are continues random variables.

Equivalent dimension – Definition: The equivalent dimension of *X* is *U=F(X)*, where *F(X)* is the cumulative distribution of *X*

Properties

- Every *U* is uniformly distributed in [0,1]
- {$U_{i=1,..p}$ } has Euclidean metric
- The distance between the two seismic events, *i, j* , is

$$d(i,j) = \sqrt{\sum_{k=1}^{p}[U_k(i) - U_k(j)]^2}$$

Technique

- The probabilistic models for earthquake parameters, $F(X_k)$, are in general not known.
- If the earthquakes' data are a representative sample of size n, replace $F(X_k)$, $k=1,..,p$ with their data-driven, kernel estimators (Silverman, 1986):

$$\hat{F}_X(x|\{x_i, n\}) = \frac{1}{n}\sum_{i=1}^{n} \Phi\left(\frac{x - x_i}{\lambda_i h}\right)$$

where: $\Phi(u)$ is the cumulative distribution function of the standard normal distribution

h is the common smoothing factor e.g. the solution of the equation (Kijko, et al., 2001):

$$\sum_{i,j}\left\{2^{-0.5}\left[\frac{(x_i - x_j)^2}{2h^2} - 1\right]exp\left[-\frac{(x_i - x_j)^2}{4h^2}\right] - 2\left[\frac{(x_i - x_j)^2}{h^2} - 1\right]exp\left[-\frac{(x_i - x_j)^2}{2h^2}\right]\right\}$$
$$= 2n$$

λ_i are the local bandwidth factors e.g.: (Orlecka-Sikora & Lasocki, 2005)

$$\lambda_i = \left[\frac{\hat{f}^*(x_i|\{x_j, n\})}{g}\right]^{-0.5}$$

$$\hat{f}^*(x_i|\{x_j, n\}) = \frac{1}{\sqrt{2\pi}hn}\sum_{j=1}^{n} exp\left[-\frac{(x_i - x_j)^2}{2h^2}\right] \qquad g = \left[\prod_{i=1}^{n}\hat{f}^*(x_i|\{x_j, n\})\right]^{\frac{1}{n}}$$

The MATLAB toolbox with codes for equivalent dimension transformation can be downloaded from https://git.plgrid.pl/projects/EA/repos/sera-applications/browse

References:

Kijko, A., Lasocki S., & Graham G. (2001) Nonparametric seismic hazard analysis in mines. *Pure and Applied Geophysis*, 158, 1655-1676.
Lasocki, S. (2014) Transformation to equivalent dimensions – a new methodology to study earthquake clustering. *Geophysical Journal International*, 197 (2), 1224-1235.
Orlecka-Sikora, B. & Lasocki, S. (2005) "Nonparametric characterization of mining induced seismic sources." In: Proceedings Sixth International Symposium on Rockburst and Seismicity in Mines 9-11 March 2005, Australia, Potvin, Y., & Hudyma, M., Eds. (Australian Centre for Geomechanics, Nedlands 2005), pp. 555-560.
Silverman, B.W. (1986) "Density Estimation for Statistics and Data Analysis" (Chapman and Hall, London, 1986).

127
128
129
130

131
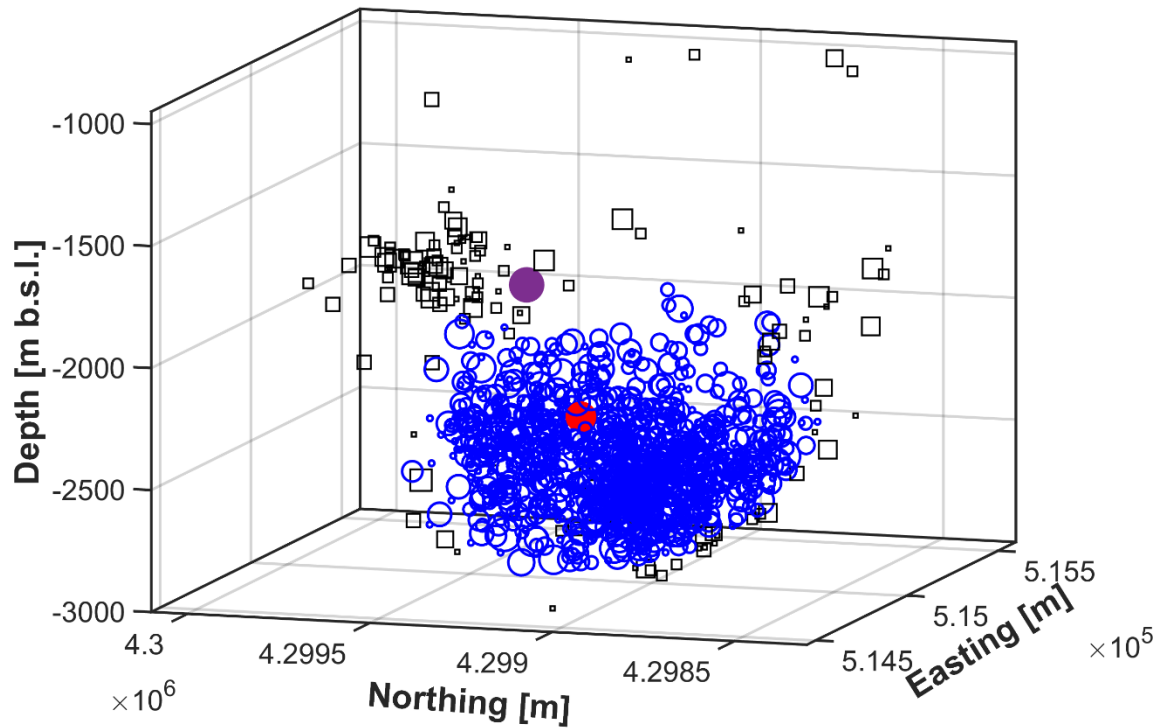
Figure S1. 3D view of spatial distribution of hypocenters of 1252 events from the seismic catalog from the NW region of The Geysers geothermal field. Blue circles indicate locations of the events from the cluster A, which have been analyzed in this paper. The other events from the initial dataset are marked by black squares. The size of markers is proportional to the magnitude of events. Big red dot marks the position of the open hole section of the Prati9 well and big violet dot marks the position of the open hole section of the Prati29 wells. The distances between the holes are: vertical – 386.8 m, horizontal – 479.5 m.
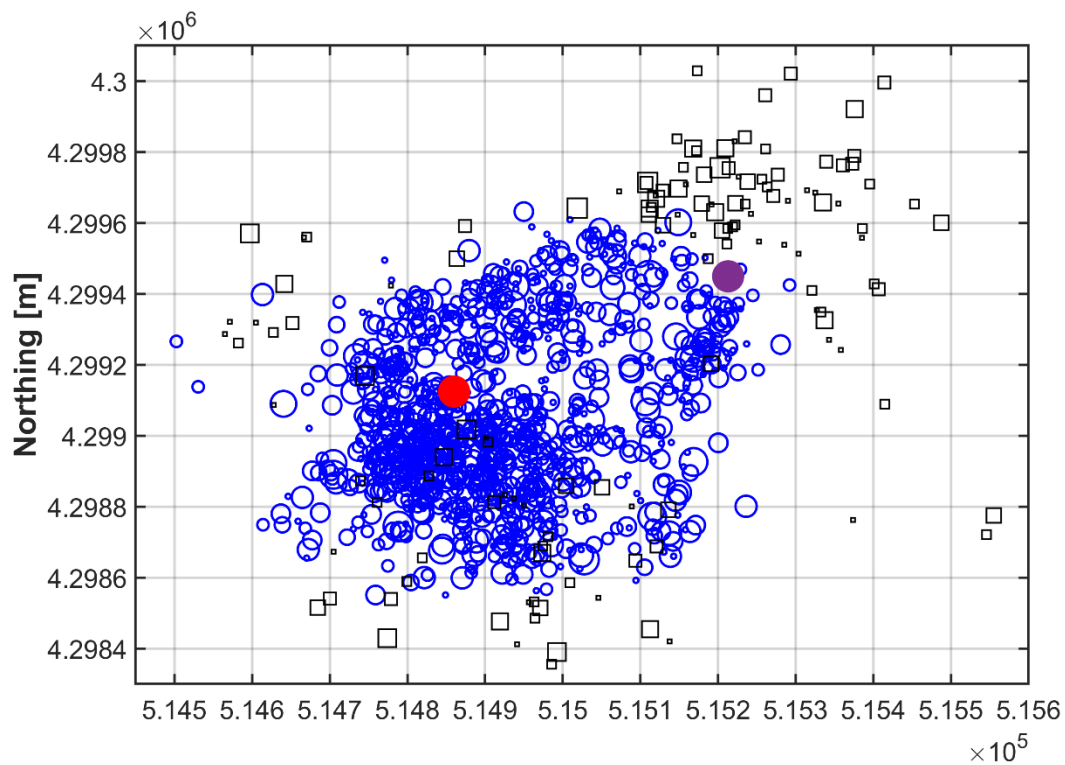
138

139
140   **Figure S2.** Horizontal projection of Figure S1.
141
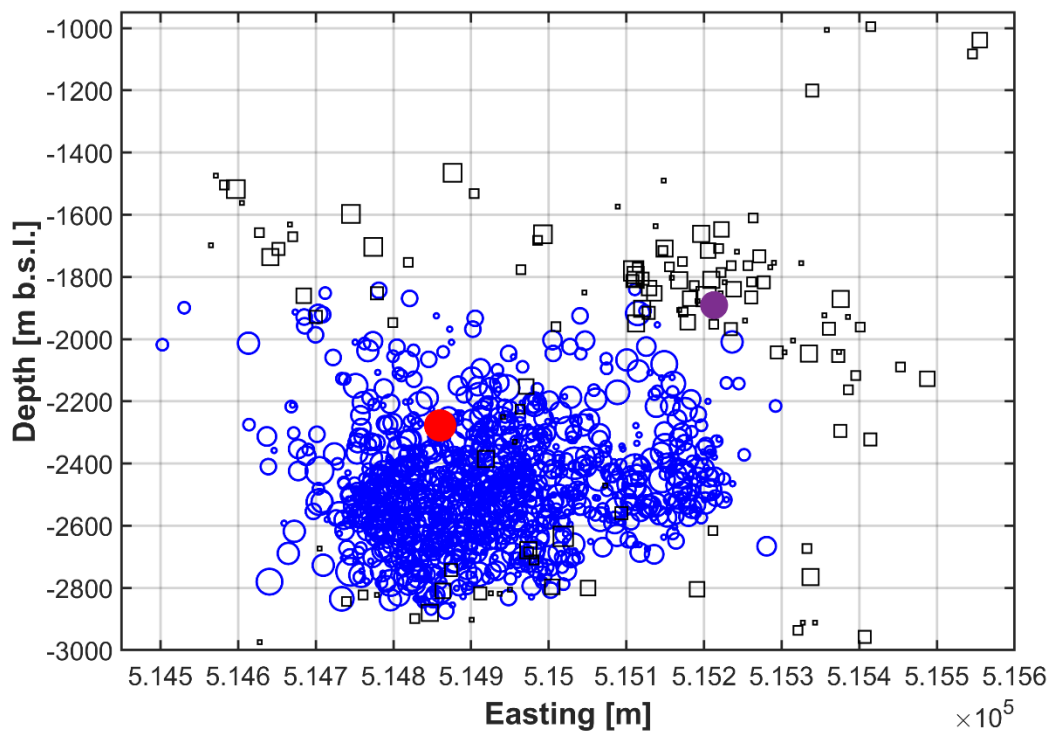
142
143   **Figure S3.** Vertical xz projection of Figure S2.
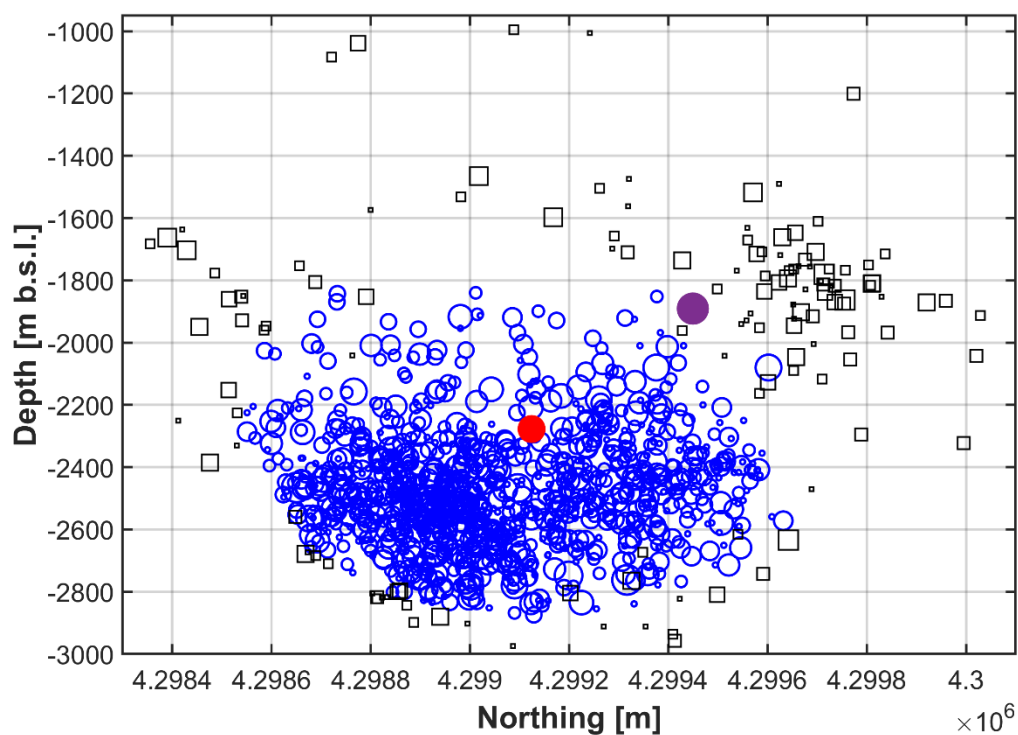
6

144
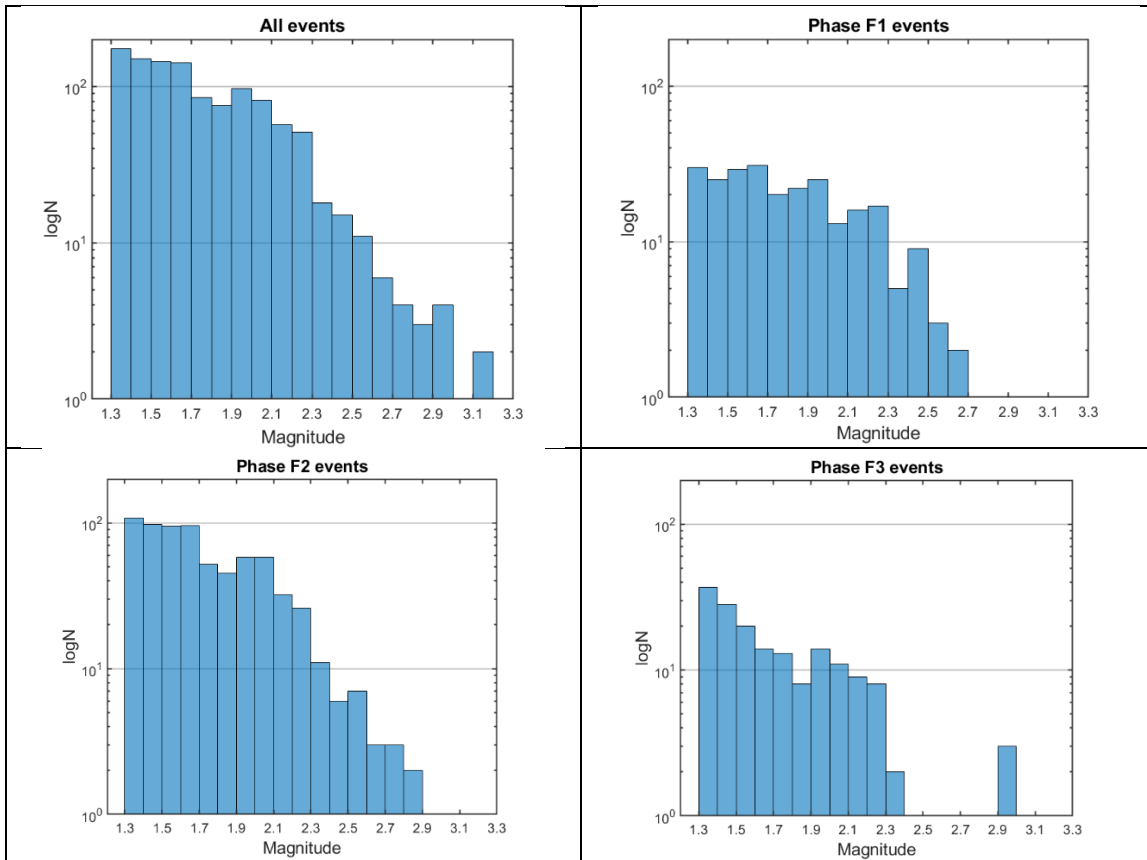**Figure S4.** Vertical yz projection of Figure S2.
145
146
147

Figure S5. Magnitude-frequency histograms of studied events
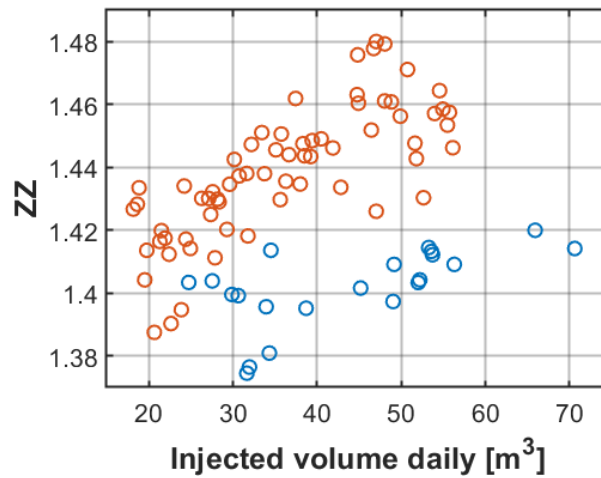

Figure S6. The degree of disordering of sources, ZZ vs. the average injection rate into Prati9 well, *IN*(9) scatterplots. Blue markers – the scatterplot for the injection phase F1. Brown markers – the scatterplot for the injection phase F2.

159 **Table S1.** Results of the correlation analysis between the average injection rate, *IN*, and the degree of
160 disordering of seismic sources, *ZZ*, and its components, $\Delta_r, \Delta_M, \Delta_\phi$ for the phase F1. The correlation have
161 been evaluated for *ZZ*, $\Delta_r, \Delta_M, \Delta_\phi$ delayed from 0 to 21 days with respect to *IN*.

Delay [days]	ZZ		Δ_r		Δ_M		Δ_ϕ	
	Corr. coef.	p-value	Corr. coef.	p-value	Corr. coef.	p-value	Corr. coef.	p-value
0	0.623	2.5E-03	0.694	4.9E-04	0.205	3.7E-01	-0.280	2.2E-01
1	0.621	2.7E-03	0.688	5.7E-04	0.210	3.6E-01	-0.275	2.3E-01
2	0.618	2.9E-03	0.682	6.6E-04	0.214	3.5E-01	-0.270	2.4E-01
3	0.614	3.0E-03	0.676	7.8E-04	0.219	3.4E-01	-0.265	2.5E-01
4	0.611	3.3E-03	0.669	9.1E-04	0.223	3.3E-01	-0.260	2.6E-01
5	0.607	3.5E-03	0.662	1.1E-03	0.227	3.2E-01	-0.255	2.6E-01
6	0.603	3.8E-03	0.654	1.3E-03	0.231	3.1E-01	-0.248	2.8E-01
7	0.599	4.1E-03	0.648	1.5E-03	0.235	3.1E-01	-0.244	2.9E-01
8	0.594	4.5E-03	0.641	1.7E-03	0.239	3.0E-01	-0.240	2.9E-01
9	0.590	4.9E-03	0.634	2.0E-03	0.243	2.9E-01	-0.236	3.0E-01
10	0.586	5.3E-03	0.627	2.3E-03	0.247	2.8E-01	-0.233	3.1E-01
11	0.581	5.7E-03	0.621	2.7E-03	0.250	2.7E-01	-0.229	3.2E-01
12	0.577	6.2E-03	0.614	3.1E-03	0.254	2.7E-01	-0.226	3.2E-01
13	0.572	6.7E-03	0.607	3.5E-03	0.257	2.6E-01	-0.223	3.3E-01
14	0.568	7.2E-03	0.602	3.9E-03	0.263	2.5E-01	-0.223	3.3E-01
15	0.563	7.8E-03	0.595	4.4E-03	0.266	2.4E-01	-0.220	3.4E-01
16	0.559	8.4E-03	0.588	5.0E-03	0.270	2.4E-01	-0.216	3.5E-01
17	0.554	9.1E-03	0.581	5.7E-03	0.274	2.3E-01	-0.213	3.5E-01
18	0.550	9.8E-03	0.574	6.5E-03	0.279	2.2E-01	-0.209	3.6E-01
19	0.545	1.1E-02	0.567	7.4E-03	0.283	2.1E-01	-0.206	3.7E-01
20	0.542	1.1E-02	0.560	8.2E-03	0.288	2.1E-01	-0.201	3.8E-01
21	0.538	1.2E-02	0.553	9.3E-03	0.292	2.0E-01	-0.198	3.9E-01

162

163 **Table S2**. Results of the correlation analysis between the average injection rate into Prati9 well, $IN(9)$, and
164 the degree of disordering of seismic sources, ZZ, and its components, $\Delta_r, \Delta_M, \Delta_\phi$ for the phase F2. The
165 correlation have been evaluated for $ZZ, \Delta_r, \Delta_M, \Delta_\phi$ delayed from 0 to 21 days with respect to $IN(9)$. The
166 results based on Spearman rank correlation are in italics.

167

Delay [days]	ZZ		Δ_r		Δ_M		Δ_ϕ	
	Corr. coef.	p-value	Corr. coef.	p-value	Corr. coef.	p-value	Corr. coef.	p-value
0	0.756	2.2E-13	0.687	1.9E-10	0.408	6.7E-04	*0.493*	*3.4E-05*
1	0.759	1.5E-13	0.693	1.1E-10	0.409	6.6E-04	*0.488*	*4.1E-05*
2	0.761	1.2E-13	0.698	7.6E-11	0.409	6.5E-04	*0.482*	*5.1E-05*
3	0.762	1.1E-13	0.701	5.8E-11	0.407	6.9E-04	*0.481*	*5.4E-05*
4	0.762	1.1E-13	0.703	4.5E-11	0.407	7.1E-04	*0.481*	*5.3E-05*
5	0.764	9.0E-14	0.707	3.1E-11	0.407	7.0E-04	*0.478*	*6.1E-05*
6	0.765	7.4E-14	0.711	2.1E-11	0.407	6.8E-04	*0.475*	*6.9E-05*
7	0.767	6.0E-14	0.715	1.5E-11	0.408	6.7E-04	*0.472*	*7.6E-05*
8	0.768	5.0E-14	0.719	1.0E-11	0.408	6.7E-04	*0.467*	*9.3E-05*
9	0.770	4.2E-14	0.723	7.0E-12	0.408	6.8E-04	*0.456*	*1.4E-04*
10	0.771	3.6E-14	0.727	4.9E-12	0.407	6.8E-04	*0.454*	*1.5E-04*
11	0.772	3.1E-14	0.730	3.6E-12	0.408	6.8E-04	*0.447*	*1.9E-04*
12	0.773	2.8E-14	0.733	2.7E-12	0.409	6.5E-04	*0.441*	*2.5E-04*
13	0.774	2.5E-14	0.736	1.9E-12	0.409	6.5E-04	*0.444*	*2.2E-04*
14	0.775	2.2E-14	0.740	1.2E-12	0.407	6.9E-04	*0.440*	*2.6E-04*
15	0.776	2.0E-14	0.743	8.7E-13	0.407	6.9E-04	*0.435*	*3.0E-04*
16	0.777	1.8E-14	0.747	6.1E-13	0.407	7.0E-04	*0.430*	*3.6E-04*
17	0.777	1.6E-14	0.750	4.4E-13	0.407	7.0E-04	*0.427*	*3.9E-04*
18	0.778	1.5E-14	0.753	3.1E-13	0.407	7.0E-04	*0.422*	*4.7E-04*
19	0.778	1.5E-14	0.755	2.5E-13	0.406	7.2E-04	*0.417*	*5.5E-04*
20	0.778	1.4E-14	0.758	1.8E-13	0.406	7.2E-04	*0.410*	*6.9E-04*
21	0.778	1.4E-14	0.760	1.4E-13	0.407	6.8E-04	*0.406*	*8.0E-04*

168

169 **Table S3**. Results of the correlation analysis between the average of total injection rate into Prati9 and
170 Prati29 wells, IN(both), and the degree of disordering of seismic sources, ZZ, and its components,
171 $\Delta_r, \Delta_M, \Delta_\phi$ for the phase F2. The correlation have been evaluated for $ZZ, \Delta_r, \Delta_M, \Delta_\phi$ delayed from 0 to
172 21 days with respect to IN(both). The results based on Spearman rank correlation are in italics.

Delay [days]	ZZ		Δ_r		Δ_M		Δ_ϕ	
	Corr. coef.	p-value	Corr. coef.	p-value	Corr. coef.	p-value	Corr. coef.	p-value
0	0.722	7.7E-12	0.663	1.3E-09	0.452	1.4E-04	*0.472*	*7.6E-05*
1	0.723	6.9E-12	0.667	9.9E-10	0.453	1.4E-04	*0.466*	*9.7E-05*
2	0.723	6.8E-12	0.668	8.6E-10	0.453	1.3E-04	*0.472*	*7.8E-05*
3	0.723	7.0E-12	0.670	7.8E-10	0.451	1.4E-04	*0.477*	*6.3E-05*
4	0.721	8.4E-12	0.669	8.0E-10	0.450	1.5E-04	*0.476*	*6.6E-05*
5	0.721	8.6E-12	0.671	7.1E-10	0.450	1.5E-04	*0.470*	*8.4E-05*
6	0.721	8.9E-12	0.672	6.5E-10	0.451	1.5E-04	*0.462*	*1.1E-04*
7	0.720	9.1E-12	0.673	5.9E-10	0.451	1.5E-04	*0.465*	*1.0E-04*
8	0.720	9.3E-12	0.675	5.3E-10	0.450	1.5E-04	*0.466*	*9.8E-05*
9	0.720	9.4E-12	0.676	4.7E-10	0.449	1.5E-04	*0.467*	*9.4E-05*
10	0.720	9.6E-12	0.677	4.2E-10	0.448	1.6E-04	*0.474*	*7.2E-05*
11	0.721	9.1E-12	0.679	3.7E-10	0.448	1.6E-04	*0.475*	*6.8E-05*
12	0.720	9.7E-12	0.679	3.6E-10	0.448	1.6E-04	*0.476*	*6.5E-05*
13	0.719	1.0E-11	0.681	3.2E-10	0.447	1.7E-04	*0.479*	*5.7E-05*
14	0.720	9.9E-12	0.684	2.5E-10	0.445	1.8E-04	*0.476*	*6.5E-05*
15	0.719	1.0E-11	0.685	2.2E-10	0.444	1.9E-04	*0.471*	*7.9E-05*
16	0.719	1.0E-11	0.687	1.9E-10	0.443	1.9E-04	*0.465*	*1.0E-04*
17	0.719	1.0E-11	0.688	1.7E-10	0.442	2.0E-04	*0.460*	*1.2E-04*
18	0.719	1.1E-11	0.690	1.5E-10	0.442	2.1E-04	*0.460*	*1.2E-04*
19	0.718	1.2E-11	0.691	1.4E-10	0.439	2.2E-04	*0.457*	*1.3E-04*
20	0.718	1.2E-11	0.692	1.2E-10	0.439	2.3E-04	*0.458*	*1.3E-04*
21	0.717	1.3E-11	0.693	1.2E-10	0.440	2.2E-04	*0.462*	*1.1E-04*

173

174 **Table S4**. Results of the correlation analysis between the average of injection rate, *IN*, and the degree of
175 disordering of seismic sources, *ZZ*, and its components, $\Delta_r, \Delta_M, \Delta_\phi$ for the phase F3. The correlation have
176 been evaluated for *ZZ*, $\Delta_r, \Delta_M, \Delta_\phi$ delayed from 0 to 21 days with respect to *IN*.

Delay [days]	*ZZ*		Δ_r		Δ_M		Δ_ϕ	
	Corr. coef.	p-value	Corr. coef.	p-value	Corr. coef.	p-value	Corr. coef.	p-value
0	-0.603	2.9E-02	-0.199	5.1E-01	-0.321	2.8E-01	-0.195	5.2E-01
1	-0.587	3.5E-02	-0.176	5.6E-01	-0.338	2.6E-01	-0.183	5.5E-01
2	-0.571	4.2E-02	-0.154	6.2E-01	-0.354	2.3E-01	-0.171	5.8E-01
3	-0.554	4.9E-02	-0.131	6.7E-01	-0.371	2.1E-01	-0.159	6.0E-01
4	-0.538	5.8E-02	-0.108	7.3E-01	-0.387	1.9E-01	-0.147	6.3E-01
5	-0.521	6.8E-02	-0.085	7.8E-01	-0.403	1.7E-01	-0.135	6.6E-01
6	-0.505	7.8E-02	-0.063	8.4E-01	-0.420	1.5E-01	-0.123	6.9E-01
7	-0.485	9.3E-02	-0.035	9.1E-01	-0.438	1.3E-01	-0.111	7.2E-01
8	-0.469	1.1E-01	-0.013	9.7E-01	-0.454	1.2E-01	-0.098	7.5E-01
9	-0.452	1.2E-01	0.009	9.8E-01	-0.471	1.0E-01	-0.085	7.8E-01
10	-0.436	1.4E-01	0.031	9.2E-01	-0.488	9.1E-02	-0.072	8.2E-01
11	-0.419	1.5E-01	0.052	8.7E-01	-0.502	8.1E-02	-0.060	8.4E-01
12	-0.402	1.7E-01	0.074	8.1E-01	-0.519	6.9E-02	-0.047	8.8E-01
13	-0.386	1.9E-01	0.096	7.6E-01	-0.535	5.9E-02	-0.033	9.2E-01
14	-0.369	2.1E-01	0.117	7.0E-01	-0.552	5.1E-02	-0.019	9.5E-01
15	-0.352	2.4E-01	0.139	6.5E-01	-0.567	4.3E-02	-0.006	9.9E-01
16	-0.335	2.6E-01	0.161	6.0E-01	-0.582	3.7E-02	0.007	9.8E-01
17	-0.317	2.9E-01	0.182	5.5E-01	-0.597	3.1E-02	0.020	9.5E-01
18	-0.299	3.2E-01	0.204	5.0E-01	-0.610	2.7E-02	0.032	9.2E-01
19	-0.281	3.5E-01	0.225	4.6E-01	-0.622	2.3E-02	0.043	8.9E-01
20	-0.264	3.8E-01	0.247	4.2E-01	-0.640	1.9E-02	0.058	8.5E-01
21	-0.245	4.2E-01	0.268	3.8E-01	-0.651	1.6E-02	0.069	8.2E-01

177

12

178 **Text S2. Comparison of the results of correlation analysis for different**
179 **representations of closeness of hypocenters.**

180   One of the three conditions which we expect to play a role in linking fractures and
181 building for-reaching pathways for fluid migration is closeness of hypocenters. This
182 condition is parameterized by the average distance between hypocenters in the space of
183 hypocenter coordinates transformed to equivalent dimension, Δ_r. The transformation to
184 equivalent dimensions was necessary to make comparable all eight used parameters of
185 seismic events: three hypocentral coordinates, three independent angles determining
186 orientations of the T and P axes of the double-couple focal mechanisms, and two angular
187 coordinates of hypocenters in the spherical system beginning at the open hole of injection
188 well. The comparability enabled, in turn, estimation of the degree of disordering of
189 seismic sources, ZZ.

190   Δ_r significantly correlated with the injection rate, IN, in the injection phases F1
191 and F2. In phase F1 Δ_r was the only one component of ZZ whose correlation with IN was
192 significant. It was then possible to apply in this phase another representations of
193 closeness of hypocenters and compare their correlation results with the ones obtained for
194 Δ_r. The metrics of distances between hypocenters in original Cartesian system is
195 Euclidean. Making use of this fact we tried correlation dimension of distances between
196 hypocenters, D_2, and summarized squared distances in the original (x,y,z) space, $d2$, as
197 alternatives to Δ_r .

198   The correlation dimension estimate, D_2 was obtained using the integral correlation
199 method (Grassberger & Procaccia, 1983; Lasocki & De Luca, 1998). D_2 is the slope of
200 the straight line, which relates the number of pairs of sources whose mutual distances are
201 smaller than a certain value of ε, with ε, in the double logarithmic scale.

202   The summarized squared distances in the original (x,y,z) space, $d2$ was
203 $\sum_{\substack{i,k \\ i \neq k}} (x_i - x_k)^2$ where $x_\bullet$ is the vector of hypocenter location in the original Cartesian
204 system of coordinates.

205   Unlike Δ_r, D_2 did not correlated with IN at the prescribed significance level
206 α=0.05. The Pearson correlation coefficient was 0.26, p=0.26. On the contrary $d2$ was
207 highly correlated with IN. The Pearson correlation coefficient was 0.87, $p=4\times10^{-7}$. We
208 also analyzed correlation between $d2$ and IN in phase F2, in which Δ_r significantly
209 correlated with IN (corr. coeff. = 0.69, $p = 2\cdot10^{-10}$, see Main text Table 2). The Pearson
210 correlation coefficient between $d2$ and IN was 0.63, $p = 2\times10^{-8}$.

211   The correlation results with $d2,$ same as those with Δ_r, validate positively the
212 results with Δ_r because $d2$ is the most basic measure of the total distance between
213 hypocenters. The reason why the correlation between D_2 and IN was not ascertained were
214 probably problems with accurate estimation of the correlation dimension of distance
215 between hypocenters, D_2. In many data widows we could not distinguish correctly the
216 linear part because the saturation and depopulation regions nearly overlapped. In the
217 below graphs we present the IN vs. correlation dimension scatterplot and two plots of the
218 correlation integral vs. threshold distance, which exemplify the difficulties with correct
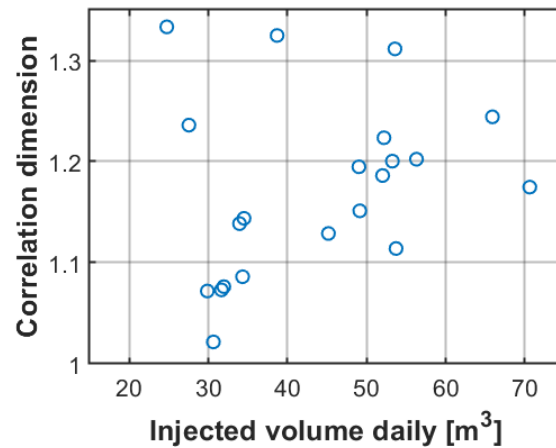219 estimation of the correlation dimension.

220
221
222 **Figure Text S2-1. Scatter plot of correlation dimension of the distance between hypocenters, D_2 vs.**
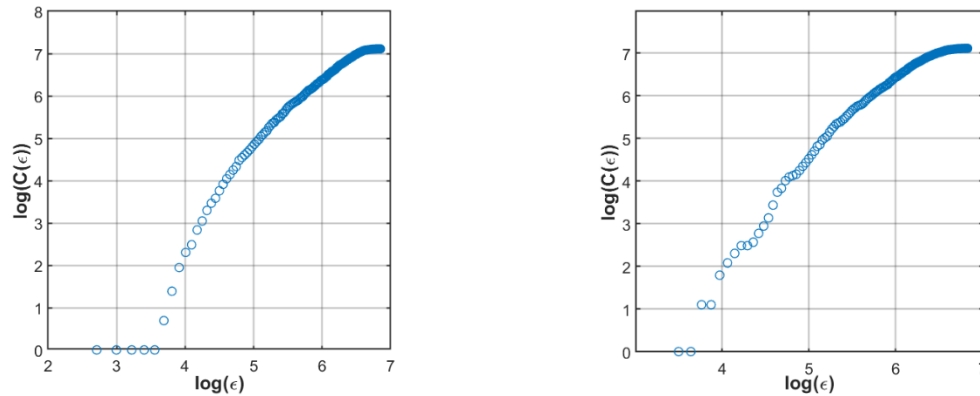223 **injected volume into Prati9 well in phase F1, $IN(9)$.**
224

225 **Figure Text S2-2. Two examples of the empirical relation between the correlation integral of the**
226 **distance between hypocenters, $C(\varepsilon)$ and the threshold distance ε.**
227
228
229 **References:**

230 Grassberger, P. & Procaccia, I. (1983) Measuring of strangeness of strange attractors.
231 *Physica D*, 9, 189–208, https://doi.org/10.1016/0167-2789(83)90298-1.
232 Lasocki, S. & De Luca, L. (1998) Monte Carlo studies of relations between fractal
233 dimensions in monofractal data sets. *Pure and Applied Geophysics*, 152, 213–220
234

235

Text S3. Discussion of the results of correlation analysis for phase F3 of injection.

In phase F3, in which the overall level of the injection rate, *IN*, was the lowest among injection phases, the correlation between *IN*, and the degree of disordering of sources, *ZZ*, was significant, negative. This correlation was achieved only jointly by the three components of *ZZ*: $\Delta_r, \Delta_M, \Delta_\phi$ because neither of the them significantly correlated with *IN* (Main text, Table 2). The negative correlation coefficient in F3 increased when *ZZ* was delayed with respect to *IN*, and for four and more days lag it became statistically not significant (Supporting Information Table S4).

The change of sign of the *IN – ZZ* correlation in F3 may be explained by the role of injection rate changes on the weakening/strengthening of rock. According to rock sample studies of Fjaer and Ruisten (2002) in rock weakening conditions there are many equivalent orientations of the failure plane, and the fracture orientation is determined by local weaknesses of the rock. In conditions of rock strengthening only two orientations for the potential failure plane fulfil the Coulomb failure criterion. Thence rock weakening conditions result in poorly ordered seismic fractures, and in rock strengthening conditions the fractures are better ordered. Orlecka-Sikora and Cielesta (2019) found two mutually reversed reactions of the stress field to injection rate changes in The Geysers, with the reversal point at some $50\text{-}70 \cdot 10^2$ m^3/day. At injection rates above this interval, increasing the injection rate enhanced rock weakening, and a decrease in the injection rate led to rock strengthening. Below this interval, the effect of injection rate variation was the opposite.

The injection rates in F1 and F2 were mostly above the aforementioned reversal point. To the contrary, the injection rates in F3 were well below this point. In the first two phases, weakening of the rock with increasing injection rate could favor the formation of randomly oriented fractures, which was expressed by the increase in the degree of disordering, *ZZ*. In F3 increasing the injection rate could lead to rock strengthening, which promoted the formation of fractures oriented in the optimal direction. As a consequence, the fractures were better ordered, which reduced *ZZ*.

We acknowledge, however, that since the data series in F3 was composed of only 13 points, the obtained *IN – ZZ* correlation (p≈0.03) might be spurious.

References:

Fjaer, E., & Ruistuen, H. (2002) Impact of the intermediate principal stress on the strength of heterogeneous rock, *Journal of Geophysical Research*, *Solid Earth*, 107, B2, 2032, doi: 10.1029/2001JB000277.
Orlecka-Sikora, B. & Cielesta, S. (2019) Evidence that the injection-induced earthquakes rupture subcritically. *Scientific Reports* (revised, under review)